Demonstration of numerical equivalence of ensemble and spectral averaging in electromagnetic scattering by random particulate media

MICHAEL I. MISHCHENKO,[1,*] JANNA M. DLUGACH,[2] AND NADEZHDA T. ZAKHAROVA[3]

[1]*NASA Goddard Institute for Space Studies, 2880 Broadway, New York, NY 10025*
[2]*Main Astronomical Observatory of the National Academy of Sciences of Ukraine, 27 Zabolotny Str., 03680, Kyiv, Ukraine*
[3]*Trinnovim LLC, 2880 Broadway, New York, NY 10025*
**Corresponding author: michael.i.mishchenko@nasa.gov*

Received XX Month XXXX; revised XX Month, XXXX; accepted XX Month XXXX; posted XX Month XXXX (Doc. ID XXXXX); published XX Month XXXX

The numerically exact superposition *T*-matrix method is used to model far-field electromagnetic scattering by two types of particulate object. Object 1 is a fixed configuration which consists of *N* identical spherical particles (with *N* = 200 or 400) quasi-randomly populating a spherical volume *V* having a median size parameter of 50. Object 2 is a true discrete random medium (DRM) comprising the same number *N* of particles randomly moving throughout *V*. The median particle size parameter is fixed at 4. We show that if Object 1 is illuminated by a quasi-monochromatic parallel beam then it generates a typical speckle pattern having no resemblance to the scattering pattern generated by Object 2. However, if Object 1 is illuminated by a parallel polychromatic beam with a 10% bandwidth then it generates a scattering pattern that is largely devoid of speckles and closely reproduces the quasi-monochromatic pattern generated by Object 2. This result serves to illustrate the capacity of the concept of electromagnetic scattering by a DRM to encompass fixed quasi-random particulate samples provided that they are illuminated by polychromatic light.

OCIS codes: *(290.5850) Scattering, particles; (030.6140) Speckle; (030.5620) Radiative transfer; (260.5430) Polarization.*

http://dx.doi.org/10.1364/JOSAA

1. INTRODUCTION

A discrete random medium (DRM) is defined as a morphologically complex object in the form of an imaginary volume *V* populated by a large number *N* of small particles in such a way that the spatial distribution of the particles throughout the volume is statistically random and uniform [1–5]. Typical examples of DRMs are natural and manmade suspensions of particles in gases and liquids. Of course at a given moment in time, the spatial distribution of particles in any multi-particle group is definite rather than random. Therefore, if the group is illuminated by a monochromatic or quasi-monochromatic parallel beam of light then statistical randomness and spatial uniformity of a DRM can be achieved only over a sufficiently long period of time as a result of random temporal changes of particle positions. This is precisely what occurs naturally in a multi-particle group suspended in a gas or a liquid and results in smooth, speckle-free patterns of time-averaged electromagnetic scattering.

The concept of a DRM is also frequently used in application to fixed particulate media such as powder surfaces, sheets of paper, layers of paint, or biological tissues. This usage is usually motivated by the non-detection of speckles in measured scattering patterns. It should be recognized, however, that in such cases the non-detection of speckles is explained by factors other than random movements of particles, for example, by the illumination of a fixed multi-particle group by a polychromatic beam [6].

Yet the smoothness of the scattering patterns measured for fixed particulate media often serves as a justification for using theoretical modeling techniques developed for true DRMs. Among such techniques are the theories of radiative transfer and weak localization derived from the macroscopic Maxwell equations (MMEs) under the explicit assumption that relevant time-averaged optical observables can be computed by averaging over a statistically uniform spatial distribution of all the particles throughout the volume *V* [1,4,5]. It is, therefore, imperative to examine whether polychromatic illumination (i.e., averaging optical observables over a finite rather than infinitesimal spectral range) can be quantitatively equivalent to averaging over random particle coordinates (i.e., ensemble averaging).

To the best of our knowledge this equivalence has never been demonstrated using controlled laboratory measurements. For practical reasons it may be more straightforward to give this demonstration using numerically exact computer solutions of the MMEs [7–9]. In fact, recent improvements in the superposition *T*-matrix method (STMM) [10,11] coupled with the current availability of efficient computer clusters make possible direct first-principle calculations of electromagnetic scattering by representative many-particle groups. Hence the main objective of this paper is to apply the modeling methodology developed in [12,13] to a quantitative analysis of whether the notion of electromagnetic scattering by a time-varying DRM can be applied to the case of polychromatic illumination of a fixed quasi-random particulate medium.

2. MODELING METHODOLOGY

For the purposes of our analysis, we will compare far-field scattering properties of two types of object. The first one (hereinafter Object 1) is a fixed *N*-particle configuration quasi-randomly populating an imaginary spherical volume having a radius *R* (Fig. 1). All particles have the same radius *r* and refractive index *m*; their coordinates are assigned using a random-number generator while making sure that the particle volumes do not overlap. The second type of object (hereinafter Object 2) is a spherical DRM whose scattering properties are modeled by taking the average of relevant optical observables over the equiprobable orientation distribution of Object 1. It has been demonstrated previously [5,12] that this type of averaging indeed yields numerical results that are essentially equivalent to those obtained by true ensemble averaging. Specifically, it has been shown that different realizations of Object 2 yield virtually indistinguishable quasi-monochromatic far-field observables. Another example of this equivalence will be discussed in Section 3.

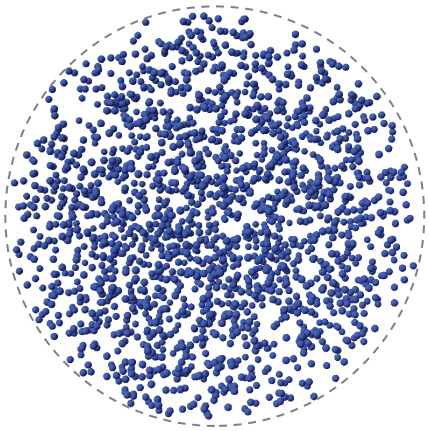

Fig. 1. A fixed *N*-particle configuration quasi-randomly populating an imaginary spherical volume.

As is well known [4,5], the transformation of the time-averaged Stokes column vector of the incident quasi-monochromatic plane wave ("inc") into the time-averaged Stokes column vector of the scattered spherical wavefront ("sca") in the far zone of a fixed object is described by the phase matrix **Z**:

$$\mathbf{I}^{\rm sca}(\rho\hat{\mathbf{n}}^{\rm sca}) = \frac{1}{\rho^2}\mathbf{Z}(\hat{\mathbf{n}}^{\rm sca},\hat{\mathbf{n}}^{\rm inc},\lambda)\mathbf{I}^{\rm inc}, \quad (1)$$

where λ is the wavelength, $\hat{\mathbf{n}}^{\rm inc} = \{\theta^{\rm inc},\varphi^{\rm inc}\}$ is the unit vector in the incidence direction, $\hat{\mathbf{n}}^{\rm sca} = \{\theta^{\rm sca},\varphi^{\rm sca}\}$ is that in the scattering direction, ρ is the distance from the center of the object to the far-zone observation point, and $\{\theta,\varphi\}$ are the zenith and azimuth angles in the fixed (laboratory) spherical coordinate system centered at the object (Fig. 2). In what follows, we will assume that $\theta^{\rm inc} = 0$.

We will consider three illumination scenarios. In the first scenario, Object 1 is illuminated by a quasi-monochromatic plane wave with a wavelength of $\lambda_0 = 2\pi/10\,\mu$m. Note that the notion and physical causes of quasi-monochromaticity of light are discussed in [14]. The corresponding normalized scattering matrix is defined as

$$\widetilde{\mathbf{F}}^{(1)}(\Theta) = C^{(1)}\mathbf{Z}(\theta^{\rm sca} = \Theta,\varphi^{\rm sca} = 0;\theta^{\rm inc} = 0,\varphi^{\rm inc} = 0;\lambda_0), \quad (2)$$

where $C^{(1)}$ is a normalization constant.

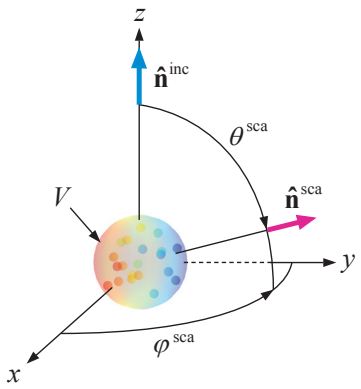

Fig. 2. Far-zone scattering geometry.

In the second scenario, Object 1 is illuminated by a polychromatic plane beam consisting of quasi-monochromatic components with wavelengths uniformly distributed over the spectral range $[0.95\lambda_0, 1.05\lambda_0]$. The 10% bandwidth is large enough to make the beam expressly polychromatic and yet small enough to be representative of many actual measurement conditions. The time-averaged Stokes column vectors of all the quasi-monochromatic components are assumed to be the same. Now the normalized scattering matrix is defined according to

$$\widetilde{\mathbf{F}}^{(2)}(\Theta) = C^{(2)}\langle\mathbf{Z}(\theta^{\rm sca} = \Theta,\varphi^{\rm sca} = 0;\theta^{\rm inc} = 0,\varphi^{\rm inc} = 0;\lambda)\rangle_\lambda, \quad (3)$$

where $\langle\cdots\rangle_\lambda$ denotes averaging over the entire spectral range in question.

In the third scenario, Object 2 is illuminated by a quasi-monochromatic plane wave with the wavelength λ_0. Furthermore, it is assumed that (i) the DRM represented by Object 2 is ergodic, and (ii) quasi-random oscillations of the incident electromagnetic field and the random changes in particle positions are statistically uncorrelated. According to Section 13.8 of [5], these assumptions imply that the corresponding time averaged normalized scattering matrix can be calculated as

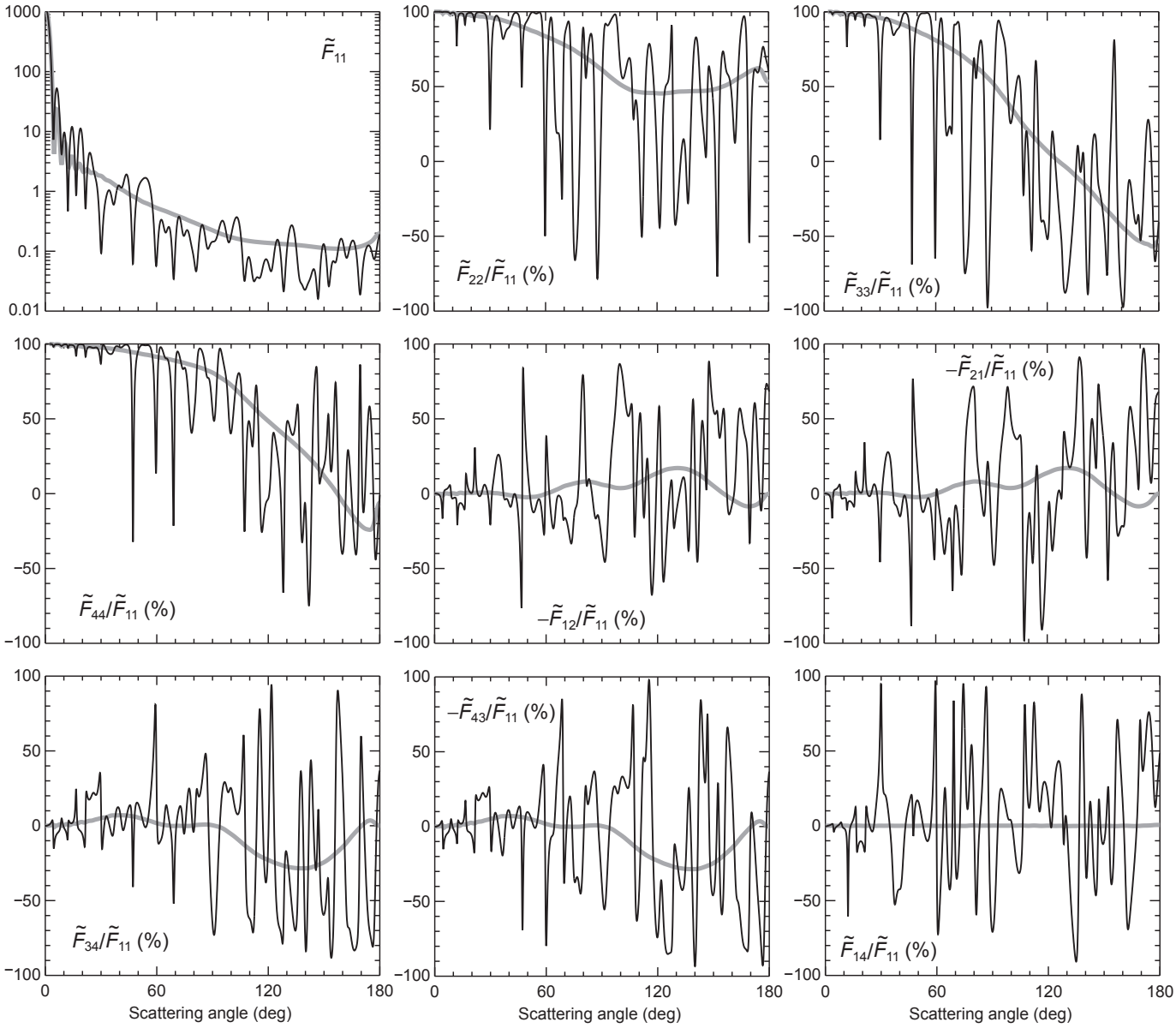

Fig. 3. Elements of the matrices $\widetilde{\mathbf{F}}^{(1)}(\Theta)$ (thin black curves) and $\widetilde{\mathbf{F}}^{(3)}(\Theta)$ (thick grey curves) for $N = 200$ and $m = 1.32$.

$$\widetilde{\mathbf{F}}^{(3)}(\Theta) = C^{(3)}\langle \mathbf{Z}(\theta^{\rm sca} = \Theta, \varphi^{\rm sca}; \theta^{\rm inc} = 0, \varphi^{\rm inc} = \varphi^{\rm sca}; \lambda_0; \Psi)\rangle_\Psi, \quad \textbf{(4)}$$

where $\langle\cdots\rangle_\Psi$ denotes ensemble averaging insofar as it is modeled by averaging over the uniform orientation distribution of Object 1 with respect to the laboratory coordinate system. Note that $\widetilde{\mathbf{F}}^{(3)}(\Theta)$ is independent of $\varphi^{\rm sca}$ because of taking the average over the uniform orientation distribution of Object 1.

The normalization constants in Eqs. (2)–(4) are chosen such that the (1,1) element in each scattering matrix (i.e., the phase function) satisfies the normalization condition

$$\frac{1}{2}\int_0^\pi {\rm d}\Theta \widetilde{F}_{11}(\Theta)\sin\Theta = 1. \quad \textbf{(5)}$$

The scattering matrices $\widetilde{\mathbf{F}}^{(1)}(\Theta)$, $\widetilde{\mathbf{F}}^{(2)}(\Theta)$, and $\widetilde{\mathbf{F}}^{(3)}(\Theta)$ are computed using the numerically exact STMM solver of the MMEs described in [11]. In all computations, R is fixed at 5 μm and r is fixed at 0.4 μm, which implies that the median size parameter of both types of particulate object is fixed at $X_0 = 2\pi R/\lambda_0 = 50$ and that of the particles is fixed at $x_0 = 2\pi r/\lambda_0 = 4$. Note that the STMM affords a quasi-analytical orientation-averaging procedure [10] that is highly efficient and accurate and yields $\widetilde{\mathbf{F}}^{(3)}(\Theta)$ results completely devoid of residual numerical noise (cf. [15]). The integration over the

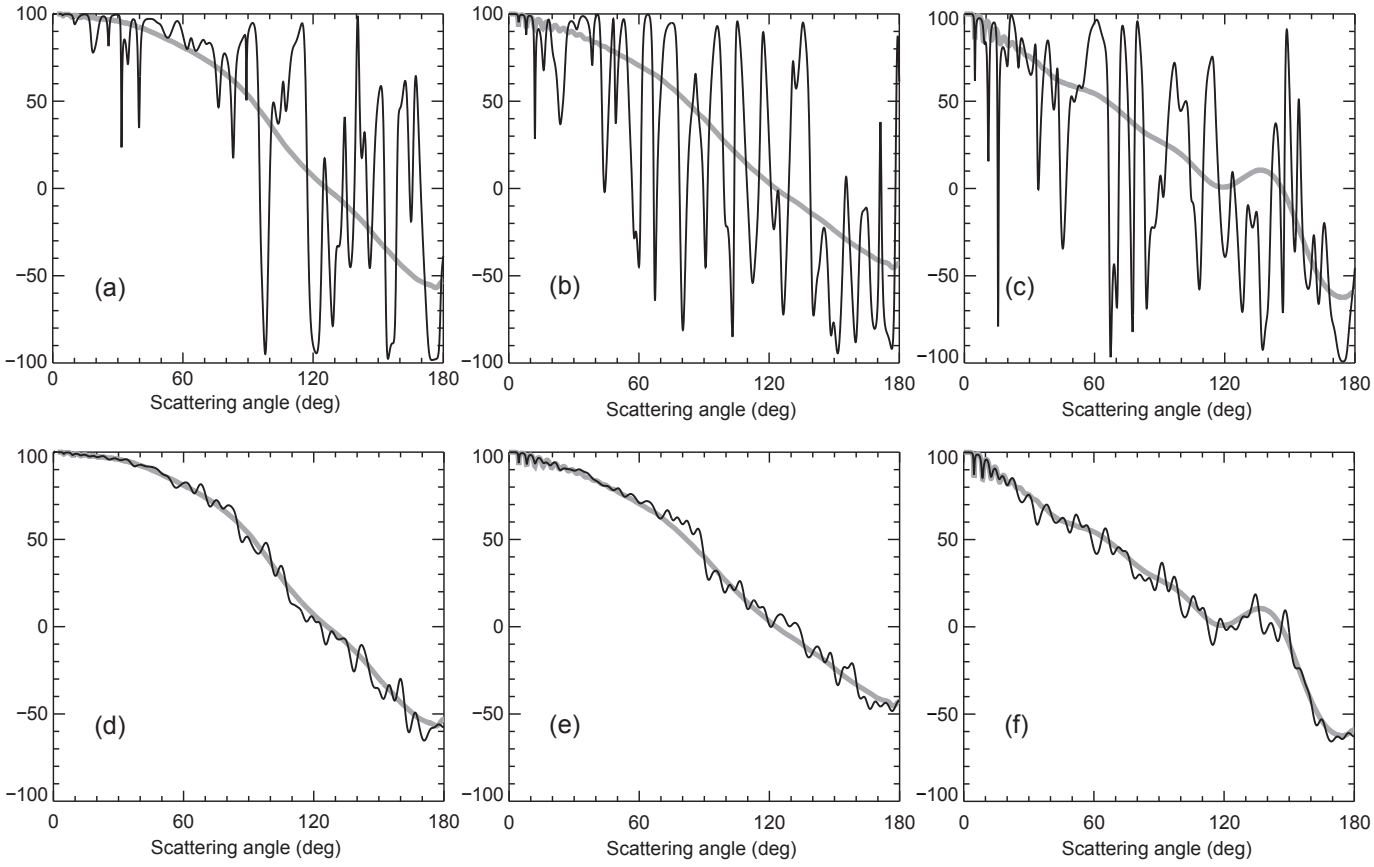

Fig. 4. Panels (a), (b), and (c) depict the ratios $\widetilde{F}_{33}^{(1)}(\Theta)/\widetilde{F}_{11}^{(1)}(\Theta)$ (thin black curves) and $\widetilde{F}_{33}^{(3)}(\Theta)/\widetilde{F}_{11}^{(3)}(\Theta)$ (thick grey curves) for different realizations of Objects 1 and 2 (see text). Panels (d), (e), and (f) are the same as panels (a), (b), and (c), respectively, except that now the thin black curves depict the corresponding ratios $\widetilde{F}_{33}^{(2)}(\Theta)/\widetilde{F}_{11}^{(2)}(\Theta)$.

spectral interval $[0.95\lambda_0, 1.05\lambda_0]$ in Eq. (3) is performed by using the Gaussian quadrature formula with 100 division points.

3. NUMERICAL RESULTS AND DISCUSSION

Owing to the uniform orientation distribution of Object 1, the dimensionless scattering matrix $\widetilde{\mathbf{F}}^{(3)}(\Theta)$ has the following well-known symmetric structure [5,16]:

$$\widetilde{\mathbf{F}}^{(3)}(\Theta) = \begin{bmatrix} \widetilde{F}_{11}^{(3)}(\Theta) & \widetilde{F}_{12}^{(3)}(\Theta) & \widetilde{F}_{13}^{(3)}(\Theta) & \widetilde{F}_{14}^{(3)}(\Theta) \\ \widetilde{F}_{12}^{(3)}(\Theta) & \widetilde{F}_{22}^{(3)}(\Theta) & \widetilde{F}_{23}^{(3)}(\Theta) & \widetilde{F}_{24}^{(3)}(\Theta) \\ -\widetilde{F}_{13}^{(3)}(\Theta) & -\widetilde{F}_{23}^{(3)}(\Theta) & \widetilde{F}_{33}^{(3)}(\Theta) & \widetilde{F}_{34}^{(3)}(\Theta) \\ \widetilde{F}_{14}^{(3)}(\Theta) & \widetilde{F}_{24}^{(3)}(\Theta) & -\widetilde{F}_{34}^{(3)}(\Theta) & \widetilde{F}_{44}^{(3)}(\Theta) \end{bmatrix}, \quad \textbf{(6)}$$

with

$$\widetilde{F}_{12}^{(3)}(0) = \widetilde{F}_{34}^{(3)}(0) = \widetilde{F}_{12}^{(3)}(\pi) = \widetilde{F}_{34}^{(3)}(\pi) = 0. \quad \textbf{(7)}$$

Our STMM computations for several realizations of Object 2 have demonstrated that the elements populating the upper right and lower left 2×2 blocks of this matrix are negligibly small (in the absolute-value sense) compared to the other elements:

$$\widetilde{\mathbf{F}}^{(3)}(\Theta) \approx \begin{bmatrix} \widetilde{F}_{11}^{(3)}(\Theta) & \widetilde{F}_{12}^{(3)}(\Theta) & 0 & 0 \\ \widetilde{F}_{12}^{(3)}(\Theta) & \widetilde{F}_{22}^{(3)}(\Theta) & 0 & 0 \\ 0 & 0 & \widetilde{F}_{33}^{(3)}(\Theta) & \widetilde{F}_{34}^{(3)}(\Theta) \\ 0 & 0 & -\widetilde{F}_{34}^{(3)}(\Theta) & \widetilde{F}_{44}^{(3)}(\Theta) \end{bmatrix}. \quad \textbf{(8)}$$

One would expect this block-diagonal structure to hold exactly for a randomly oriented scattering object with a plane of symmetry [5,16]. Strictly speaking, a multi-particle object such as the one shown in Fig. 1 does not have a plane of symmetry. Yet by virtue of being composed of a large number of quasi-randomly positioned particles it probably possesses at least one quasi-plane of symmetry, which could explain Eq. (8).

There is no *a priori* reason to expect the matrix $\widetilde{\mathbf{F}}^{(1)}(\Theta)$ to have the same block-diagonal structure as well as satisfy Eq. (7). Figure 3 (computed for N = 200 and m = 1.32) shows indeed that the element $\widetilde{F}_{14}^{(1)}(\Theta)$ does not vanish, the element $\widetilde{F}_{21}^{(1)}(\Theta)$ is distinctly different from the element $\widetilde{F}_{12}^{(1)}(\Theta)$, and there is little resemblance between the elements $\widetilde{F}_{34}^{(1)}(\Theta)$ and $-\widetilde{F}_{43}^{(1)}(\Theta)$. Furthermore, the elements $\widetilde{F}_{12}^{(1)}(\Theta)$, $\widetilde{F}_{21}^{(1)}(\Theta)$, $\widetilde{F}_{34}^{(1)}(\Theta)$, and $\widetilde{F}_{43}^{(1)}(\Theta)$ substantially deviate from zero at

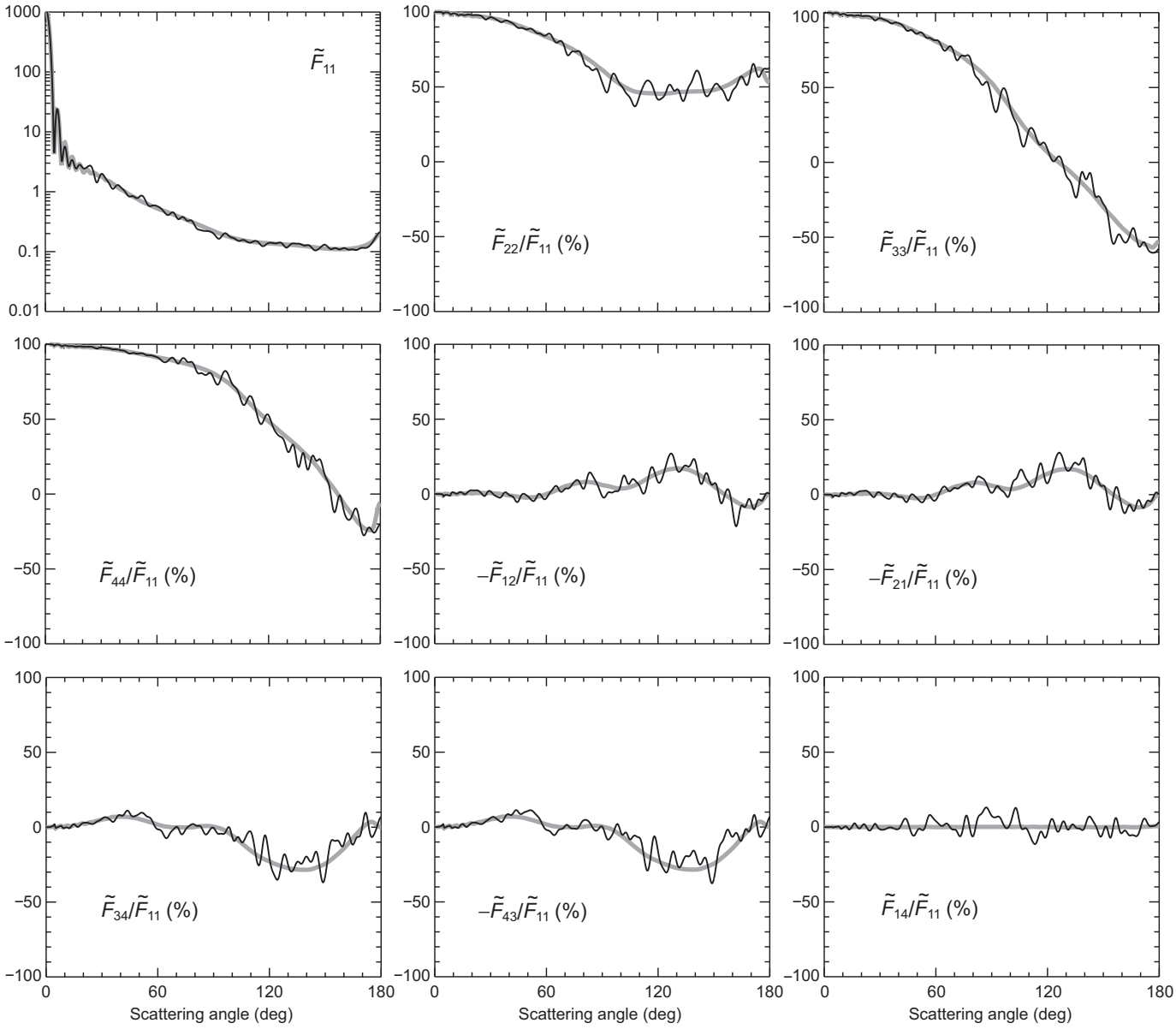

Fig. 5. As in Fig. 3, but for the matrices $\widetilde{\mathbf{F}}^{(2)}(\Theta)$ (thin black curves) and $\widetilde{\mathbf{F}}^{(3)}(\Theta)$ (thick grey curves).

$\Theta = \pi$. Most importantly, all $\widetilde{\mathbf{F}}^{(1)}(\Theta)$ curves in Fig. 3 reveal quasi-irregular large-amplitude oscillations which exemplify the famous speckle phenomenon typical of fixed objects illuminated by a collimated monochromatic or quasi-monochromatic beam [6,17].

In a stark contrast, the corresponding ensemble-averaged $\widetilde{\mathbf{F}}^{(3)}(\Theta)$ curves satisfy Eq. (7) and—to a high numerical accuracy—Eq. (8), are completely devoid of speckles, and illustrate smooth scattering patterns typical of a true time-varying DRM [5,12].

Furthermore, a change in particle positions of Object 1 changes the speckles in the $\widetilde{\mathbf{F}}^{(1)}(\Theta)$ angular patterns completely, while leaving the corresponding matrix $\widetilde{\mathbf{F}}^{(3)}(\Theta)$ essentially intact. This is illustrated in Fig. 4(a) computed by switching the sign of the z-coordinates of the particles forming Object 1 in Fig. 3. In fact, the practical indistinguishability of all $\widetilde{F}_{11}^{(3)}(\Theta)$ and $\widetilde{F}_{ij}^{(3)}(\Theta)\big/\widetilde{F}_{11}^{(3)}(\Theta)$ curves for this alternative realization of Object 2 from those for the original one (not shown here) illustrates once again that averaging over all orientation of a quasi-randomly generated Object 1 simulates very well the true ensemble averaging.

Similarly dramatic changes in the $\widetilde{\mathbf{F}}^{(1)}(\Theta)$ patterns occur when the number of particles increases from N = 200 to N = 400 (Fig. 4(b)) or when the particle refractive index increases from m = 1.32 to m = 1.6 (Fig. 4(c)). Yet the corresponding $\widetilde{\mathbf{F}}^{(3)}(\Theta)$ curves remain quite smooth and speckle free.

All these traits of the matrices $\widetilde{\mathbf{F}}^{(1)}(\Theta)$ and $\widetilde{\mathbf{F}}^{(3)}(\Theta)$ show unequivocally that the latter is representative of a DRM whereas the former is not.

Figure 5 reveals a dramatically different picture. It is seen that averaging over wavelengths has three pronounced effects. First, it drastically suppresses the speckles and yields much smoother scattering-matrix curves. Second, the structure of the matrix $\widetilde{\mathbf{F}}^{(2)}(\Theta)$ is now well described by Eqs. (7) and (8). Third, although there is residual small-amplitude "noise", the overall angular profiles of the $\widetilde{\mathbf{F}}^{(2)}(\Theta)$ curves essentially coincide with the corresponding $\widetilde{\mathbf{F}}^{(3)}(\Theta)$ curves. These effects appear to be quite robust, as illustrated by comparing the top panels of Fig. 4 with their bottom counterparts.

To explain the above STMM results qualitatively, let us assume that the spatial distribution of particles in Fig. 1 is so sparse that each particle is located in the far zones of all the other particles. In this case the exact integral-equation counterparts of the MMEs, called the Foldy equations, can be replaced by the algebraic far-field Foldy equations, as described in Chapter 6 of [5]. Then the scattered electromagnetic field in the far zone of the entire multi-particle group can be expressed as an infinite series of terms, each representing the contribution from an ordered n-particle sequence with $n \geq 1$. The Stokes column vector (1) of the total scattered field can then be expressed as the sum of an infinite number of terms, each representing the result of interference of two spherical wavelets centered at the end particles of a pair of ordered particle sequences.

Two such ordered particle sequences, with n = 4 and 3, are shown in Fig. 6. If the interference of the corresponding pair of spherical wavelets at the distant observation point is constructive (destructive) then it serves to increase (decrease) the total intensity scattered in the direction $\hat{\mathbf{n}}^{\text{sca}}$. As a consequence, the pair of particle sequences contributes either a bright or a dark spot to the speckle pattern generated by the entire multi-particle group.

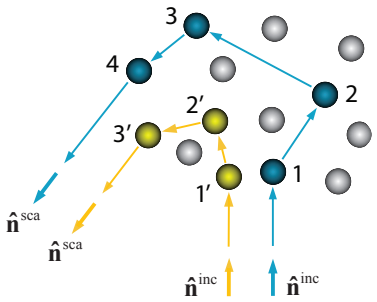

Fig. 6. Interference origin of speckles generated by a sparse fixed multi-particle group.

It is straightforward to show that the result of the interference of the wavelets generated by two ordered particle sequences depends largely on the complex exponential factor $\exp(\mathrm{i}\Delta)$, where $\mathrm{i} = (-1)^{1/2}$ and Δ is the phase difference between the corresponding light paths. In the case of the two light paths shown in Fig. 6,

$$\Delta = (2\pi/\lambda)(r_4 + R_{43} + R_{32} + R_{21} + \hat{\mathbf{n}}^{\text{inc}} \cdot \mathbf{R}_1 - r_{3'} - R_{3'2'} - R_{2'1'} - \hat{\mathbf{n}}^{\text{inc}} \cdot \mathbf{R}_{1'}), \quad (9)$$

where r_i is the distance from particle i to the observation point, R_{ij} is the interparticle distance, and $\mathbf{R}_i$ is the position vector of particle i with respect to the laboratory coordinate system. In general, random changes of particle coordinates in a DRM cause frequent temporal oscillations of the factor $\exp(\mathrm{i}\Delta)$. As a consequence, only the contributions from certain types of pairs of particle sequences survive time averaging and cause prominent optical phenomena typical of DRMs such as the forward-scattering interference, the diffuse background, and coherent backscattering [5,12]. All three phenomena are best seen in the resulting phase function $\widetilde{F}_{11}^{(3)}(\Theta)$ (the upper left panel of Fig. 3) in the form of the strong forward-scattering peak, featureless side scattering, and a narrow backscattering maximum.

In a fixed multi-particle configuration such as that shown in Fig. 1, the coordinates of the particles do not change. However, it is obvious from Eq. (9) that another efficient way of randomizing the factor $\exp(\mathrm{i}\Delta)$ is to scan a range of wavelengths. This explains qualitatively why the wavelength-averaged matrix $\widetilde{\mathbf{F}}^{(2)}(\Theta)$ in Figs. 4(d)–4(f) and 5 exhibits the same overall traits as those typical of the ensemble-averaged matrix $\widetilde{\mathbf{F}}^{(3)}(\Theta)$ computed for a true time-varying DRM.

The residual small-amplitude noise in the $\widetilde{\mathbf{F}}^{(2)}(\Theta)$ curves and the complete lack thereof in the $\widetilde{\mathbf{F}}^{(3)}(\Theta)$ curves could be explained by the smaller average range of $\Delta/2\pi$ values in the case of averaging over wavelengths for a relatively small particulate volume. Indeed, it is a large number of oscillations of the factor $\exp(\mathrm{i}\Delta)$ that serves to reduce the residual noise. If so, this noise can be expected to weaken and ultimately disappear with increasing X_0 and N.

4. CONCLUDING REMARKS

In view of Eq. (9) and the accompanying discussion, it may not be exceedingly surprising that a fixed, quasi-random particulate medium illuminated by a polychromatic parallel beam exhibits qualitatively the basic scattering traits of a true DRM. What is surprising is the numerical near identity of the respective scattering patterns despite the large values of the packing density (10% for N = 200 and 20% for N = 400). The numerical closeness of the $\widetilde{\mathbf{F}}^{(2)}(\Theta)$ and $\widetilde{\mathbf{F}}^{(3)}(\Theta)$ curves in Figs. 4(d)–4(f) and Fig. 5 cannot be explained by simple qualitative arguments based on the far-field Foldy equations and could only be revealed via direct, numerically exact solutions of the MMEs. Yet this result appears to be fundamentally important since it allows for the generalization of the notion of electromagnetic scattering by a DRM to encompass not only time-varying particulate media but also fixed quasi-random multi-particle configurations provided that the latter are illuminated by polychromatic light.

The suppression of speckles in Figs. 4(d)–4(f) and Fig. 5 appears to give credence to the widespread use of the radiative transfer theory and its *ad hoc* modifications to model "diffuse multiple scattering" by fixed particulate layers illuminated by polychromatic beams. One should remember however that this

theory is explicitly based on the far-field Foldy equations [4,5] and as such may be inapplicable to particulate samples with packing densities exceeding a few percent [18–20].

The 10% bandwidth of the polychromatic beam used in our simulations can be larger than that in many actual experiments. However, the typical size parameter of real particulate samples is also much greater than 50, which implies that the resulting range of variability of Δ in Eq. (9) should be sufficiently large for our main conclusions to hold.

Finally we note that polychromatic illumination is not the only factor potentially causing the suppression of the observed speckle pattern. Among other factors are the use of detectors of light with poor angular resolution and illumination by uncollimated incident beams [6] (e.g., Gaussian beams [21]). It should be quite instructive to extend our work by modeling the effects of these factors—as well as their combinations with spectral averaging—on the speckle patterns generated by fixed particulate samples. Yet another factor can be a macroscopic movement of a rigid particulate sample as a whole relative to the source of light and/or the detector during the measurement. This movement also can result in dramatic quasi-random changes of the $\exp(i\Delta)$ factors and cause the suppression of the resulting speckle pattern, thereby revealing—at least in a qualitative sense—the typical diffuse and coherent-backscattering regimes [22–24]. This last factor can be especially important in remote-sensing applications (see, e.g., [25–27]).

Funding Information. NASA Remote Sensing Theory Program; National Academy of Sciences of Ukraine via the Main Astronomical Observatory GRAPE/GPU/GRID Computing Cluster Project.

Acknowledgment. We thank three anonymous reviewers for helpful suggestions. Numerous insightful discussions with Daniel Mackowski, Karri Muinonen, Antti Penttilä, Viktor Tishkovets, and Gorden Videen are greatly appreciated. We also thank Antti Penttilä for providing Fig. 1.

References

1. A. Ishimaru, *Wave Propagation and Scattering in Random Media* (Academic, 1978).
2. L. Tsang, J. A. Kong, and R. T. Shin, *Theory of Microwave Remote Sensing* (Wiley, 1985).
3. L. Tsang, J. A. Kong, and K.-H. Ding, *Scattering of Electromagnetic Waves: Theories and Applications* (Wiley, 2000).
4. M. I. Mishchenko, L. D. Travis, and A. A. Lacis, *Multiple Scattering of Light by Particles: Radiative Transfer and Coherent Backscattering* (Cambridge University, 2006). http://www.giss.nasa.gov/staff/mmishchenko/books.html
5. M. I. Mishchenko, *Electromagnetic Scattering by Particles and Particle Groups: An Introduction* (Cambridge University, 2014).
6. J. W. Goodman, *Speckle Phenomena in Optics: Theory and Applications* (Roberts & Company, 2007).
7. M.I. Mishchenko, W. J. Wiscombe, J. W. Hovenier, and L. D. Travis, Overview of scattering by nonspherical particles, in *Light Scattering by Nonspherical Particles: Theory, Measurements, and Applications*, M. I. Mishchenko, J. W. Hovenier, and L. D. Travis, eds., Academic (2000), pp. 29–60.
8. F. M. Kahnert, "Numerical methods in electromagnetic scattering theory," J. Quant. Spectrosc. Radiat. Transfer **79–80**, 775–824 (2003).
9. M. Kahnert," Numerical solutions of the macroscopic Maxwell equations for scattering by non-spherical particles: a tutorial review," J. Quant. Spectrosc. Radiat. Transf., in press (2016).
10. D. W. Mackowski and M. I. Mishchenko, "Calculation of the *T* matrix and the scattering matrix for ensembles of spheres," J. Opt. Soc. Am. A **13**, 2266–2278 (1996).
11. D. W. Mackowski and M. I. Mishchenko, "A multiple sphere *T*-matrix Fortran code for use on parallel computer clusters," J. Quant. Spectrosc. Radiat. Transfer **112**, 2182–2192 (2011).
12. M. I. Mishchenko, L. Liu, D. W. Mackowski, B. Cairns, and G. Videen, "Multiple scattering by random particulate media: exact 3D results," Opt. Express **15**, 2822–2836 (2007).
13. J. M. Dlugach, M. I. Mishchenko, L. Liu, and D. W. Mackowski, "Numerically exact computer simulations of light scattering by densely packed, random particulate media," J. Quant. Spectrosc. Radiat. Transfer **112**, 2068–2078 (2011).
14. A. Lipson, S. G. Lipson, and H. Lipson, *Optical Physics* (Cambridge University, 2011).
15. F. Voit, J. Schäfer, and A. Kienle, "Light scattering by multiple spheres: comparison between Maxwell theory and radiative-transfer-theory calculations," Opt. Lett. **34**, 2593–2595 (2009).
16. H. C. van de Hulst, *Light Scattering by Small Particles* (Wiley, 1957).
17. J. C. Dainty, ed., *Laser Speckle and Related Phenomena* (Springer, 1975).
18. A. Ishimaru, and Y. Kuga, "Attenuation constant of a coherent field in a dense distribution of particles," J. Opt. Soc. Am. **72**, 1317–1320 (1982).
19. K. Muinonen, M. I. Mishchenko, J. M. Dlugach, E. Zubko, A. Penttilä, and G. Videen, "Coherent backscattering verified numerically for a finite volume of spherical particles," Astrophys. J. **760**, 118 (2012).
20. M. I. Mishchenko, D. Goldstein, J. Chowdhary, and A. Lompado, "Radiative transfer theory verified by controlled laboratory experiments," Opt. Lett. **38**, 3522–3525 (2013).
21. D.W. Mackowski and M.I. Mishchenko, "Direct simulation of multiple scattering by discrete random media illuminated by Gaussian beams," Phys. Rev. A **83**, 013804 (2011).
22. S. Etemad, R. Thompson, and M. J. Andrejco, "Weak localization of photons: universal fluctuations and ensemble averaging," Phys. Rev. Lett. **57**, 575–578 (1986).
23. M. Kaveh, M. Rosenbluh, I. Edrei, and I. Freund, „Weak localization and light scattering from disordered solids," Phys. Rev. Lett. **57**, 2049–2052 (1986).
24. R. Lenke and G. Maret, "Multiple scattering of light: coherent backscattering and transmission," in *Scattering in Polymeric and Colloidal Systems*, W. Brown and K. Mortensen, eds., Gordon and Breach (2000), pp. 1–73.
25. M. I. Mishchenko and J. M. Dlugach, "Coherent backscatter and the opposition effect for E-type asteroids," Planet. Space Sci. **41**, 173–181 (1993).
26. M. I. Mishchenko, "On the nature of the polarization opposition effect exhibited by Saturn's rings," Astrophys. J. **411**, 351–361 (1993).
27. Yu. G. Shkuratov, K. Muinonen, E. Bowell, K. Lumme, J. I. Peltoniemi, M. A. Kreslavsky, D. G. Stankevich, V. P. Tishkovets, N. V. Opanasenko, and L. Y. Melkumova, "A critical review of theoretical models of negatively polarized light scattered by atmosphereless solar system bodies," Earth Moon Planets **65**, 201–246 (1994).